Journal of Hydrology 540 (2016) 574–587

Contents lists available at ScienceDirect

Journal of Hydrology

journal homepage: www.elsevier.com/locate/jhydrol

Applications of a thermal-based two-source energy balance model using Priestley-Taylor approach for surface temperature partitioning under advective conditions

Lisheng Song [a,b], William P. Kustas [b,*], Shaomin Liu [a,*], Paul D. Colaizzi [c], Hector Nieto [b,d], Ziwei Xu [a], Yanfei Ma [e], Mingsong Li [f], Tongren Xu [a], Nurit Agam [g], Judy A. Tolk [c], Steven R. Evett [c]

[a] State Key Laboratory of Remote Sensing Science, and School of Geography, Beijing Normal University, Beijing 100875, China
[b] U.S. Department of Agricultural, Agricultural Research Service, Hydrology and Remote Sensing Lab, Beltsville, MD 20705, USA
[c] U.S. Department of Agricultural, Agricultural Research Service, Conservation and Production Research Laboratory, P.O. Drawer 10, Bushland, TX 79012, USA
[d] Institute for Sustainable Agriculture (IAS), Spanish Research Council (CSIC), Campus Alameda Del Obispo, Av. Menéndez Pidal S/n, 14004 Córdoba, Spain
[e] Department of Geography, Handan College, Hebei 056005, China
[f] School of Resources and Environment, University of Electronic Science and Technology of China, Chengdu 611731, China
[g] Jacob Blaustein Institutes for Desert Research, Ben-Gurion University of the Negev, Sede Boqer Campus 84990, Israel

ARTICLE INFO

Article history:
Received 22 March 2016
Received in revised form 5 June 2016
Accepted 13 June 2016
Available online 16 June 2016
This manuscript was handled by Tim R. McVicar, Editor-in-Chief, with the assistance of Di Long, Associate Editor

Keywords:
Evaporation and transpiration
Two-Source Energy Balance
Evapotranspiration
Stable isotopic method
Lysimeter
Microlysimeter

ABSTRACT

In this study ground measured soil and vegetation component temperatures and composite temperature from a high spatial resolution thermal camera and a network of thermal-IR sensors collected in an irrigated maize field and in an irrigated cotton field are used to assess and refine the component temperature partitioning approach in the Two-Source Energy Balance (TSEB) model. A refinement to TSEB using a non-iterative approach based on the application of the Priestley-Taylor formulation for surface temperature partitioning and estimating soil evaporation from soil moisture observations under advective conditions (TSEB-A) was developed. This modified TSEB formulation improved the agreement between observed and modeled soil and vegetation temperatures. In addition, the TSEB-A model output of evapotranspiration (*ET*) and the components evaporation (*E*), transpiration (*T*) when compared to ground observations using the stable isotopic method and eddy covariance (*EC*) technique from the HiWATER experiment and with microlysimeters and a large monolithic weighing lysimeter from the BEAREX08 experiment showed good agreement. Difference between the modeled and measured *ET* measurements were less than 10% and 20% on a daytime basis for HiWATER and BEAREX08 data sets, respectively. The TSEB-A model was found to accurately reproduce the temporal dynamics of *E*, *T* and *ET* over a full growing season under the advective conditions existing for these irrigated crops located in arid/semi-arid climates. With satellite data this TSEB-A modeling framework could potentially be used as a tool for improving water use efficiency and conservation practices in water limited regions. However, TSEB-A requires soil moisture information which is not currently available routinely from satellite at the field scale.

1. Introduction

Evapotranspiration (*ET*) and its partitioning between evaporation (*E*) and transpiration (*T*) is a significant component of the water and energy cycle at all scales, from field and watershed to regional and global, and is essential to many applications in climate, weather, hydrology, and ecology (Seneviratne et al., 2010). Research suggests that *T* is likely to account for about 65% of continental *ET* (including rainfall interception by the vegetation) (Good et al., 2015; Zhang et al., 2016), in order to maintain a mass balance between plant transpiration and CO_2 uptake (Jasechko et al., 2013). In irrigated agriculture, quantification and management of *ET* and its components, *E* and *T*, is essential for reliable irrigation scheduling, quantifying recharge and drainage, and yield forecasting (Zhu et al., 2014). However, validation of models computing relative contributions of *E* and *T* is rare owing to the difficulties in measuring *E* and *T* even at the field scale (Agam et al., 2012; Colaizzi et al., 2012a; Jasechko et al., 2013).

Norman et al. (1995) and Kustas and Norman (1999) developed a two-source energy balance model (TSEB) using land surface

* Corresponding authors.
E-mail addresses: Bill.Kustas@ARS.USDA.GOV (W.P. Kustas), smliu@bnu.edu.cn (S. Liu).

http://dx.doi.org/10.1016/j.jhydrol.2016.06.034
0022-1694/

temperature as a key boundary condition for computing reliable daytime sensible and latent heat fluxes of the soil and canopy elements for partially-vegetated land surfaces. In the original TSEB formulation of Norman et al. (1995), both a series resistance and a parallel resistance approach were derived. However the series resistance approach is often used instead of the parallel approach, since the former allows for interaction between the soil and the canopy and is generally found to be more robust (Song et al., 2015).

In the TSEB scheme, the canopy transpiration component of the latent heat flux is approximated using the modified form of the Priestley-Taylor approach. This is motivated by its simplicity for large scale operational applications and the apparent robustness of its prediction. Then combining a simple linear unmixing method based on the Stefan–Boltzmann law between the emitted blackbody radiation and temperature, the canopy and soil component temperatures are separated from the composite radiometric temperature observation. Finally, the latent heat fluxes from soil and canopy elements are derived using the flux-gradient analogy to Ohm's law and energy conservation principles for the soil-plant-atmosphere continuum.

The TSEB model and its revisions have been integrated into a regional modeling system for computing surface energy fluxes operationally over a wide variety of vegetation, and climates using satellite data (Anderson et al., 2011). In the TSEB scheme, the Priestley-Taylor coefficient α_{PT} for the vegetated canopy is normally set to an initial value of $\alpha_{PT} \sim 1.26$, but is incrementally reduced to account for water-limited conditions. Briefly, when negative soil evaporation results, then the α_{PT} value is reduced and fluxes and temperatures are recomputed in an iterative procedure until a soil latent heat flux value greater than zero is computed (Anderson et al., 2012; Kustas et al., 2012). However, increasing α_{PT} under well-watered advective conditions cannot be done iteratively based on model solutions for the soil and canopy latent heat (LE) fluxes or temperatures (Kustas and Norman, 1999; Agam et al., 2010) and so there is no direct way of accounting for strongly advective conditions *a priori* with this type of formulation. Even without advection, semiarid and arid climates typically have large diurnal variation in vapor pressure deficit, which is not accounted for using a constant α_{PT} value (Long and Singh, 2012). This may result in T being underestimated, forcing E/ET to be overestimated, because initial estimates of canopy and soil temperature are over- and underestimated, respectively. Colaizzi et al. (2012a, 2014) showed that this could be mitigated by replacing the Priestley-Taylor with the Penman-Monteith formulation in TSEB. However, the Penman-Monteith formulation requires accurate humidity measurements (to calculate vapor pressure deficit), which are not always available at large scales or where vegetation is heterogeneous. Consequently, more comprehensive validation studies of soil and vegetation temperatures and E and T are needed at the field scale in order to assess current and any future refinements to the TSEB formulations.

How accurately the current version of TSEB model partitions E and T from ET under different environmental conditions requires validation with ground measurements of E and/or T, while the paucity of datasets having component fluxes and temperature measurements hinders the assessment of TSEB for ET partitioning (Song et al., 2015, 2016; Yang et al., 2013a, 2015). The errors in E and T may be compensating so that discrepancies in the total LE or ET are minor in comparison (Colaizzi et al., 2012a). A few studies have estimated T from sap-flow measurements (Wu et al., 2006); however, this method can only provide daily transpiration estimates (Yang et al., 2013b) and measurements are limited to the scale of individual plants, which imposes limitations in upscaling to the field level because spatial variability is likely in vegetation and soil conditions. E can be measured using microlysimeters where the average weight losses are directly proportional to evaporation (Colaizzi et al., 2012a; Song et al., 2015).

Another approach, a novel flux partitioning approach, that requires only standard eddy covariance instrumentation and relies upon a limited number of assumptions for its theoretical development has been proposed (the correlation-based partitioning approach: (Scanlon and Kustas, 2010, 2012)). However, independent E and T measurements are needed in concert with the eddy covariance measurements to rigorously validate this method.

Recently, based on the theory of that E from soil and T from plants each contribute unique isotopic signals to water vapor within the ecosystem boundary layer (Williams et al., 2004), some studies have partitioned E and T by measurements of the isotopic composition of oxygen in soil, plants and atmospheric water vapor (Kool et al., 2014). This method has been implemented successfully not only at canopy scale but also at catchment scale (Hu et al., 2014; Jasechko et al., 2013; Williams et al., 2004; Zhang et al., 2011). However it also has limitations, such as uncertainty in the measurement of the isotopic signals of ET, T and E, which can produce a ten-fold level of uncertainty in T/ET values (Hu et al., 2014; Wen et al., 2016).

The objective of this study is to modify the TSEB model to account for the advection without tuning Priestley-Taylor parameter for partitioning soil and vegetation temperatures from a composite radiometric surface temperature, to estimate ET and its partitioning E and T under significant advective conditions. This modified TSEB model for advective conditions (TSEB-A) avoids the need to adjust α_{PT} parameter for the canopy elements under high vapor pressure deficit (VPD) conditions, but where sufficient available water is present in the soil profile. We hypothesize that this approach may also reduce the errors in estimating canopy and soil temperatures, and consequently estimates of E and T.

2. Methodology

2.1. Two-source energy balance model (TSEB)

The TSEB modeling scheme originally proposed by Norman et al. (1995) has undergone several revisions, improving the radiation partitioning between the soil and canopy (Colaizzi et al., 2012a, 2012b), the soil surface aerodynamic resistance to heat transport, the effect of vegetation clumping on resistances and radiation divergence (Kustas and Norman, 1999), or the replacement of Priestley-Taylor with the Penman-Monteith formulation (if humidity measurements are available) (Colaizzi et al., 2014). The TSEB model partitions the composite surface radiometric temperature, measured by a sensor viewing at an angle θ, into soil and canopy component temperatures, T_s and T_c, based on the fraction of vegetation cover f_c (θ) observed by the sensor, using the Stefan-Boltzmann law, which relates a blackbody temperature to radiance emission (Kustas and Norman, 1999; Norman et al., 1995). Then the derived T_s and T_c are used to calculate the surface energy balance for the soil and canopy components of the composite land-surface system (Kustas et al., 2012).

The soil and vegetation net radiation R_{ns} and R_{nc}, respectively, are estimated using the method proposed by Kustas and Norman (1999). Their formulations are as follows:

$$Rn_s = \tau_{longwave} L_{\downarrow} + (1 - \tau_{longwave})\varepsilon_c \sigma T_c^4 - \varepsilon_s \sigma T_s^4 + \tau_{solar}(1 - a_s) S_{\downarrow} \quad (1)$$

$$Rn_c = (1 - \tau_{longwave})(L_{\downarrow} + \varepsilon_s \sigma T_s^4 - 2\varepsilon_c \sigma T_c^4) + (1 - \tau_{solar})(1 - a_c) S_{\downarrow}. \quad (2)$$

where $S_{\downarrow}$ and $L_{\downarrow}$ are the incoming shortwave and longwave radiation from the sky, respectively, in W m^{-2}; a_s and a_c are the soil and vegetation albedo, respectively. Furthermore, $\tau_{longwave}$ and τ_{solar} are the longwave and shortwave radiation transmittances through the

canopy, respectively. ε_s and ε_c are the emissivities of soil and canopy elements.

Surface soil heat flux (G_0) is often calculated as a constant fraction of Rn_s or Rn. However, G_0 and Rn_s can be strongly out of phase for some soils. Therefore, G_0 was calculated using the model of Santanello and Friedl (2003):

$$G_0 = Rn_s\left\{a \cdot \cos\left[\frac{2\pi}{b}(t+c)\right]\right\} \tag{3}$$

where t is the solar time angle (s), and a, b, and c are empirical constants (a = 0.30, b = 80,000 s, and c = 3600 s; (Colaizzi et al., 2012a).

To allow for the interaction between the soil and canopy fluxes, the series version of TSEB is most often used to estimate the land surface fluxes. The formulations for the H_s, H_c, and their sum (H) are expressed as:

$$H_s = \rho C_p \frac{T_s - T_{ac}}{r_s} \tag{4a}$$

$$H_c = \rho C_p \frac{T_c - T_{ac}}{r_x} \tag{4b}$$

$$H = \rho C_p \frac{T_{ac} - T_a}{r_{ah}} \tag{4c}$$

where ρ is the air density (kg m^{-3}), C_p is the specific heat of air (J kg^{-1} K^{-1}), T_{ac} is the air temperature in the canopy layer (K), r_s is the resistance to heat flow in the boundary layer immediately above the soil surface (s m^{-1}), r_x is the total boundary layer resistance of the complete canopy leaves (s m^{-1}).

In TSEB, an initial calculation of T_c has usually used a form of the Priestley-Taylor equation (Priestley and Taylor, 1972), which was proposed by Norman et al. (1995) and has been validated both with measurements and complex soil-vegetation-atmosphere-tra nsfer (SVAT) schemes (Kustas and Anderson, 2009) as well as over strongly advective environments (Anderson et al., 2012; Kustas et al., 2012).

$$LE_c = \alpha_c f_G \frac{\Delta}{\Delta+\gamma} Rn_c \tag{5}$$

Using the parallel resistance formulation for ease and simplicity for an initial computation of canopy temperature, the following expression is derived;

$$T_{ci} = T_a + \frac{Rn_c r_{AH}}{\rho C_p}\left[1 - \alpha_c f_G \frac{\Delta}{\Delta+\gamma}\right] \tag{6}$$

where T_{ci} is the initial estimate of T_c, T_a is the air temperature at the reference height, r_{AH} is the aerodynamic resistance (s m^{-1}) to turbulent heat transport between the canopy source height. The α_c is the Priestley-Taylor coefficient for the canopy and its value for the canopy transpiration under non-stressed conditions is assumed to be ~1.26 derived empirically by Priestley and Taylor (1972), f_G is the fraction of green vegetation which is able to transpire, Δ is the slope of the saturation vapor pressure versus air temperature curve (kPa K^{-1}) and γ is the psychrometric constant of ~0.06 kPa K^{-1}. The value of f_G can be estimated using remote sensing (Donohue et al., 2008; Fisher et al., 2008; Guzinski et al., 2013) or can be extracted from ground measured digital images in local applications (Liu et al., 2013). Given the derived T_c, T_s is calculated from the composite radiometric surface temperature at the specified view angle ($T_{rad}(\theta)$) and the fraction of vegetation coverage ($f_c(\theta)$), emissivities of land surface (ε), vegetation (ε_c) and soil (ε_s), as following equation,

$$T_{rad}^4(\theta)\varepsilon = f_c(\theta)\varepsilon_c T_c^4 + [1 - f_c(\theta)]\varepsilon_s T_s^4 \tag{7}$$

Under canopy stress conditions, using a α_c value of ~1.26 can result in an underestimated canopy temperature, which then results in deriving an elevated T_s-from Eq. (7) and causes $H_s > Rn_s - G_0$ and hence $LE_s < 0$; under daytime conditions $LE_s < 0$ is clearly not a physical solution. Under such conditions, the TSEB model iteratively reduces the initial α_c until $LE_s > 0$ (see Anderson et al. (2005) and Li et al. (2005) for details).

2.2. Modified two-source energy balance model (TSEB-A)

Under well-watered conditions, TSEB is initialized using $\alpha_c \sim 1.26$ but under extremely advective conditions where vapor pressure deficits of ~4 kPa or larger exist, α_c appears to be larger (Agam et al., 2010). Furthermore, the difficulty in adjusting (increasing) the α_c values for advective conditions may lead to an overestimate of E relative to T (Colaizzi et al., 2014).

Under high vegetation cover combined with advective conditions, the iteration procedure in TSEB described above may not be necessary, particularly since the model has no iterative mechanism to increase α_c beyond the standard value of 1.26. As an alternative to the iterative approach, energy limited soil evaporation can also be modeled in terms of the available energy at the soil surface, and the soil limited evaporation can be adjusted by a factor related to soil wetness (f_{sw}).

$$LE_s = f_{sw}\alpha_s \frac{\Delta}{\Delta+\gamma}(Rn_s - G_0) \tag{8}$$

where f_{sw} is the factor of soil water stress which is used to adjust soil evaporation under drier surface conditions, and α_s is the Priestley-Taylor coefficient applied to the soil. Then applying the parallel resistance formulation for the soil sensible heat flux as in Norman et al. (1995) together with (Eq. (6)) again to compute soil sensible heat flux, the equation for estimating T_{si} is the following:

$$T_{si} = T_a + \frac{(r_{si} + r_{AH})}{\rho C_p}\left[(Rn_s - G_0)\cdot\left(1 - f_{sw}\alpha_s\frac{\Delta}{\Delta+\gamma}\right)\right] \tag{9}$$

where r_{si} is similar to r_s, but here computed using the original formulation soil resistance equation proposed for the TSEB model (Norman et al., 1995) that does not require estimates of T_s and T_c, and all other terms are as defined previously.

The α_s and α_c are respectively expressed according to Tanner and Jury (1976) and Agam et al. (2010):

$$\alpha_s = \begin{cases} 1 & \tau \leqslant \tau_0 \\ \alpha_{PT} - \frac{(\alpha_{PT}-1)(1-\tau)}{1-\tau_0} & \tau > \tau_0 \end{cases} \tag{10}$$

$$\alpha_c = \begin{cases} \frac{(\alpha_{PT}-\alpha_s\tau)}{(1-\tau)} & \tau \leqslant \tau_0 \\ 1.26 & \tau > \tau_0 \end{cases} \tag{11}$$

where α_{PT} = 1.26 for energy limited conditions, τ is the fraction of net radiation that reached the soil surface, which is computed using leaf area index (LAI) and a canopy extinction coefficient of radiation (Campbell and Norman, 1998). The variable τ_0 is the critical value below which the canopy cover is sufficiently dense for soil evaporation to approach equilibrium ($\alpha_s \approx 1$ for wet soil conditions); for this study a value τ_0 = 0.2 was assumed (Agam et al., 2010). The available soil water was near field capacity in the two field sites due to frequent irrigation during the growing season. The crops were assumed to be under non-stressed conditions and therefore α_c = 1.26 (Liu et al., 2016).

The value of f_{sw} can be calculated using surface soil water content (0–10 cm) according to Campbell and Norman (1998):

$$f_{sw} = \frac{2}{1 + (\theta/\theta_0)^{-2}} \tag{12}$$

where θ is the volumetric water content and θ_0 is for the water content at field capacity, which is soil-type dependent and assumed $\theta_0 \sim 0.3$ for the soils in this study area. If f_w great than 1, it is set

to 1. After applying the Priestly-Taylor formulation on soil and canopy surface, respectively, the soil and vegetation temperatures can be derived separately using Eqs. (6) and (9), respectively. This approach can avoid the uncertainties introduced by the iteration process using the Priestley-Taylor coefficient α_c which may exceed the initial value of 1.26 under the advective conditions. However, this technique does require an estimate of the surface soil moisture which is not routinely available at field scale using remote sensing. On the other hand, disaggregation techniques applied to microwave satellite remote sensing soil moisture products may provide reasonable estimates for more uniform landscapes (Merlin et al., 2013). Given the soil and vegetation temperatures, the heat fluxes from the soil and canopy can be derived directly with the following equation

$$H = \rho C_p \frac{T_{ac} - T_a}{r_A} \quad (13)$$

where r_A is the aerodynamic resistance between the air-canopy layer ($m\,s^{-1}$) and it was calculated according to Kustas and Norman (1999). Then the latent heat fluxes from the soil and vegetation surface are solved using their energy balance equation, respectively. Although the component temperatures are derived using the parallel resistance network which is computationally easy and efficient, the series resistance formulation for computing H is used since solutions tend to be more stable under high vegetation cover conditions although solutions using either the parallel or series resistance formulation generally yield similar results (Li et al., 2006).

3. Materials

The two study sites selected to evaluate the performance of the TSEB-A model were located in irrigated agricultural areas under strongly advective conditions (1): the Zhangye, located in the middle of Heihe River Basis (HiWATER, Gansu Province, China (100°22′E, 38°51′N; 1556 m above sea level) containing irrigated maize fields; and (2) the Bushland, TX study area (BEAREX08), located west of Amarillo, Texas, United States (35°11′N, 102°06′E, 1170 m above sea level) containing irrigated and rainfed cotton fields. For HiWATER, a total of 1863 observations (n = 1863) from 98 days over the growing season were used and for BEAREX08 n = 589 from 28 days of observations during the growing season.

In the HiWATER study area, the annual average air temperature and precipitation were 7.3 °C and 130.4 mm, respectively, and the main precipitation period is from June to September. However, the average annual potential evaporation is as high as 2002.5 mm (1971–2000) (measured by Chinese micro-pans (McVicar et al., 2007)). The soil type is silt clay loam on the surface and silt loam in the deeper layer (Zhu et al., 2014). Here, the tower-based flux observation systems at Daman Superstation were constructed in May 2012 at this site belonging to the Multi-Scale Observation Experiment on Evapotranspiration over heterogeneous land surfaces, which was part of the Heihe Water Allied Telemetry Experimental Research (HiWATER-MUSOEXE) (Li et al., 2013; Xu et al., 2013). The sensible and latent heat fluxes were measured at 4.5 m above the maize covered ground by an eddy covariance (EC) system, which consists of an open-path infrared gas analyzer (Li-7500A, LiCor Inc., Lincoln,[1] Nebraska, USA) and a 3-D sonic anemometer (CSAT3, Campbell Scientific Inc., Logan, Utah, USA), with a sampling frequency of 10 Hz using a data logger (CR1000, Campbell Scientific Inc., Logan, Utah, USA). The recoded raw data were processed using the Edire software (http://www.geos.ed.ac.uk/abs/-research/micromet/EdiRE/) and finally averaged over 30 min (Liu et al., 2011, 2013). The uncertainties in H and LE observations were investigated during the HiWATER-MUSOEXE by Wang et al. (2015) and were found to be ~20% for H and ~15% for LE, which are within the widely accepted accuracies for the EC measurements (Richardson et al., 2006).

Ancillary hydro-meteorological measurements included air temperature and relative humidity (model AV-14TH, Avalon Scientific, Inc., Somerton, Somerset, UK), and wind speed/direction (model Windsonic, Gill Instruments Limited., Lymington, Hampshire, UK) at 3, 5, 10, 15, 20, 30, 40 m above ground level (agl) with a sampling frequency of 10 s, and 10 min averages. A tipping bucket rain gauge (model TE525MM, Campbell Scientific, Inc., Logan, Utah, USA) was installed at the height of 2.5 m agl that was about 8 m away from the meteorological tower. The downward and upward solar and longwave radiation were measured at the height of 12 m agl from a four-component radiometer (model PSP & PIR, Eppley Laboratory, Inc., Newport, Rhode Island, USA). Soil moisture and temperature (model CS616, Campbell Scientific, Inc., Logan, Utah, USA) at 0.02, 0.04, 0.1, 0.2, 0.4, 0.8, 1.2 and 1.6 m under the ground were measured. Three plates (model HFP01SC, Hukseflux Thermal Sensors, Delftechpark, Delft, Netherlands) were located 0.06 m below ground to measure the soil heat fluxes with one buried under a maize plant along the row and the other two plates were buried under bare soil between the maize plants. These data were logged every 10 min by a digital micrologger equipped with an analog multiplexer used for sampling and logging data. Then the surface soil heat fluxes (G_0) were calculated using the vegetation fraction of the three heat-plates measurements, combined with the PlateCal approach proposed by Liebethal et al. (2005). Finally, leaf area index (LAI) was estimated using a LiCor LAI-2000 canopy analyzer (PCA, Li-Cor, Lincoln, Nebraska, USA) and while the fraction of vegetation and green vegetation coverage were estimated from digital photography collected during the experiment. The plant width, plant height, leaf width and leaf length were measured on the ground at regular spacing plots. The soil and vegetation emissivities were estimated from a hand portable remote sensing FT-IR spectrometer (model 102 F, Designs & Prototypes Ltd, Simsbury, Connecticut, USA) and applying the Iterative Spectrally Smooth Temperature Emissivity Spectrometer (ISSTES) model to ground observation (Mu et al., 2013).

A Fluke Ti55 thermal infrared camera with spectral ranges from 8 to 14 μm (Fluke Corporation, Everett, Washington, USA) which was manually operated with a view zenith angle less than 60° on a 25-m-high platform on a flux tower in the Daman superstation, measured the thermal radiation of the cropland. The images with resolution less than 0.03 m including visible spectral (VIS) and thermal infrared (TIR) radiances were recorded by the camera approximately every 120 min from 07:00 to 19:00 China Standard Time (CST) during daytime, and for each time interval, eight images including four VIS and four TIR were collected by facing north, east, south and west. After co-registering the VIS and TIR images, high resolution VIS images can be directly classified into soil and vegetation pixels using a maximum-likelihood supervised classification method. Then the brightness temperatures recorded by the TIR images were converted to surface radiometric temperature according to the radiative transfer equation, combining the ground measured atmospheric down-welling radiation and emissivities of soil and vegetation. Finally, the mean soil and vegetation temperatures were derived as the average surface temperature for soil and vegetation pixels respectively, according to the VIS image classification results. Details of this procedure can be found in Zhou et al. (2015b).

The derived soil and canopy temperatures were evaluated indirectly. Firstly, they were converted to composite land surface

[1] Mention of company or trade names is for description only and does not imply endorsement by the Beijing Normal University and US Department of Agriculture. The USDA is an equal opportunity provider and employer.

temperatures using the measured vegetation fractional cover and component emissivities. Then these composite temperatures derived using Eq. (7) were compared to the radiometric temperatures estimated from the downwelling and upwelling long-wave radiation measured by the four-component radiometer (Zhou et al., 2015a) which resulted in a likely uncertainty on the order of 1.0 K (Li et al., 2014). The estimated composite surface temperatures were analyzed on selected days according to the weather and crop conditions and when stable oxygen and hydrogen isotopes measurements were available. Table 1 shows the details of crop cover/LAI and environment conditions from the ground measurements. The first two days (DOY170 and 173) correspond to early in the growing season while the second two days are near the peak biomass (DOY 192 and 195) where LAI values reach a maximum, and the last three days (DOY 231, 252 and 256) are later in the season with the crop undergoing senescence.

Statistical measures used were mean bias error (MBE) of modeled-observed composite temperature, root-mean-square-error (RMSE) and mean absolute percent difference (MAPD), which is the mean absolute difference between modeled and observed divided by the mean observed value multiplied by 100. In comparing the composite temperatures derived from the thermal camera with the upwelling longwave radiation-derived (hemispherical) temperatures MB/RMSE values for the north, south, and east viewing were 0.26/1.60 K, 0.31/1.62 K, and 0.91/1.62 K, respectively, while the west viewing had slightly larger values with the MB/RMSE of 0.92/1.82 K. A comparison of the mean "estimated" composite surface temperature from the four orientations with the thermal camera versus the hemispherical radiometric temperature observations are illustrated in Fig. 1.

Table 1
Mean values of vegetation growth and environment conditions during the selected seven days.[a]

	LAI	ET (mm)	Wind speed (s/m)	Air temperature (K)	VPD (kPa)	Solar radiation (W/m^2)
DOY170	1.68	4.56	1.48	297.68	2.00	644
DOY173	2.13	5.29	1.31	300.96	2.71	754
DOY192	4.43	6.73	0.75	300.01	2.13	748
DOY195	4.43	6.70	0.66	299.29	2.02	772
DOY231	3.32	5.75	1.01	296.33	1.49	705
DOY252	2.97	4.86	1.09	298.46	2.16	633
DOY256	2.93	3.73	1.19	286.85	0.93	648

[a] *ET* was measured from EC system, air temperature VPD and Solar radiation (downwelling) measured from automatic weather station (AWS).

To partition *ET* into *E* and *T* on the ground by using the isotopic method, the quantification of each isotopic composition of *ET*, *E* and *T* must be derived respectively. To determine the three parameters in this study, an isotropic analyzer measured $\delta^{18}O$ of atmospheric water vapor and their flux ratios (L1102-I, Picarro Inc, Santa Clara, California, USA) at the Daman Superstation during the HiWATER-MUSOEXE. Details of the isotope experiment are given by Huang and Wen (2014). The schematic diagram of the isotope analyzer, its principle of operation, and its calibration procedure are described elsewhere (Wen et al., 2012, 2016; Huang and Wen, 2014). Briefly, the flux isotopic ratio of *ET* was determined by the flux gradient approach using the vertical gradients of water isotopic at two observing heights above the canopy (Huang and Wen, 2014; Lee et al., 2007). Given the measured $\delta^{18}O$ of atmospheric water vapor and their flux ratios, the isotopic ratio of *E* was computed using the Craig-Gordon model (Williams et al., 2004) and that of *T* was approximated under assumption of isotopic steady state, according to the $\delta^{18}O$ of xylem water. Finally the ratios of *E* and *T* in the ecosystem *ET* can be calculated based on the conservation principles, while the isotopic composition of *ET*, *E* and *T* were determined. Details on upscaling the partitioning of *ET* into *E* and *T* field scale using the isotopic approach is given by Hu et al. (2014) and Wen et al. (2016). In brief it involved sampling leaves from different levels or height of one maize plant, as well as stem and soil samples. The sampling occurred over the 13:00–15:00 (CST) period every 2 or 3 days from one sampling plot and then water in these solid samples were extracted and their isotope ratios were determined using liquid water isotope analyzer (Model DLT-100, Los Gatos Research, California, USA). In addition, since the ground observations of δ_{ET}, δ_E, δ_T can be affected by rainfall, irrigation and strong advection (Huang and Wen, 2014), 16% the ground measured data around these events were removed from the analyses.

The Bushland Evapotranspiration and Agricultural Remote sensing Experiment (BEAREX08) was conducted at the USDA-ARS Conservation & Production Research Laboratory Bushland, Texas (35°11′N, 102°06′E, 1170 m above sea level). Additional details of the BEAREX08 field campaign are described in Evett et al. (2012b), but a summary of the measurements used in this study is given here. The site is also located with a semi-arid region with a high evaporative demand up to 2600 mm per year and limited precipitation averaging 470 mm per year, with strong advection of heat energy from the south and southwest that usually contributes to abundant evapotranspiration demand. Upland cotton (*Gossypium hirsutum* L.) was planted on raised beds and irrigated by a lateral-move sprinkler system to fully meet crop

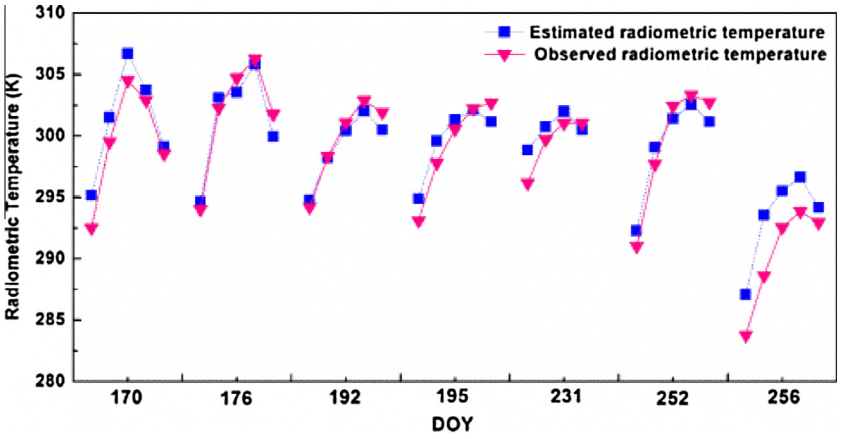

Fig. 1. Comparison of composite land surface temperature from the thermal-IR camera measurements and procedure defined in the text (estimated composite temperature) versus land surface temperature from the longwave sensor (observed hemispherical composite temperature) on selected days.

ET. Measurements from June 16 to September 24 (DOY 178–267) were applied to evaluate the TSEB-A model. During this period the crop fields transitioned from essentially bare soil conditions to nearly fully vegetated and subsequent vegetation senescence.

ET was measured by a large monolithic weighing lysimeter (nominally 3 × 3 m wide and 2.4-m deep) (model SM-50, Interface Scottsdale., Arizona, USA) located in the center of each irrigated cotton fields, the present study including lysimeter measurements were conducted in the northeast (NE) field, detailed description of the lysimeter are given by Marek et al. (1988) and the lysimeter was calibrated and found to have an absolute accuracy to within 0.04 mm/h, or equivalently 27 W/m^2 (Evett et al., 2012c). However during the early growth stage of the cotton, the cotton biomass with the lysimeter differed from the surrounding field which resulted in a tendency to overestimated field *ET* (Alfieri et al., 2012; Evett et al., 2012c; Kustas et al., 2015). To measure *E* from the soil surface, 10 microlysimeters divided in two equal replicates were deployed across two inter-rows, and spaced 0.075, 0.25, 0.375, 0.525 and 0.675 m west to east adjacent to the lysimeter. Surface radiometric temperature was measured using two infrared thermometers (model IRT/c, Exergen Corp., Watertown, Massachusetts, USA) deployed 1.5 m agl with the radiometers having a nadir view. The microlysimeters were manually weighted at sunrise and sunset using an electronic scale with a precision of 0.1 g (equal to 0.01 mm of water) in an enclosed box to avoid wind effects on the measurements (Agam et al., 2012). Meteorological data required by TSEB-A model including solar radiation (model PSP & PIR, Eppley Laboratory,Inc., Newport, Rhode Island, USA), wind speed (model Wind Sentry 03101-5, R. M. Young Co., Traverse City, Michigan, USA), air temperature and relative humidity (model HMP45C, Vaisala, Inc., Helsinki, Finland) were acquired from a standard meteorological station about 250 m east of the lysimeter. In addition, soil heat flux was measured at the lysimeter by four plates (HFT-1, Radiation and Energy Balance System, Inc., Seattle, Washington, USA) deployed at 5 cm depth and along with copper-constantan thermocouples (TMTSS-125G, Omega Engineering, Inc., Stamford, Connecticut, USA) and soil moisture sensors (CS616, Campbell Scientific, Inc., Logan, Utah, USA) deployed at 1 and 4 cm below the soil surface. These plates-thermocouple sets were deployed with two of them beneath adjacent crop rows and other two beneath adjacent inter-rows. Surface soil heat flux was computed using the calorimetric method, which included measurements of volumetric soil water content to calculate the volumetric heat capacity of the soil in two layers above the soil heat flux plates (Evett et al., 2012a). The soil water content measurements were at ~5 cm using Hydra-probes nearby and at similar positions in the inter-row and row as the soil heat flux measurements.

Plant measurements including leaf area index (model Li-3100, Lincoln, Nebraska, USA), canopy height and row width were collected periodically at key growth stages at sites in the vicinity of the lysimeters. The time series of these parameters were derived by using a linear interpolation as a function of time based on growing degree days (Colaizzi et al., 2012a).

Table 2
Statistical results of modeled versus measured soil and vegetation component temperatures using original TSEB formulation versus TSEB-A.

	Measured (K)		TSEB-A (K)		TSEB (K)	
	Tc	*Ts*	*Tc*	*Ts*	*Tc*	*Ts*
Mean value	298.32	301.35	297.98	301.31	298.59	301.62
SD	3.77	5.25	4.20	4.551	5.26	7.37
Mean bias			−0.34	−0.24	0.27	0.27
RMSE			1.50	2.72	1.60	5.78

4. Results

4.1. Evaluation of modeled soil and canopy temperatures and fluxes using TSEB and TSEB-A with HiWATER data

The agreement between observed and modeled temperatures using TSEB-A is generally better than TSEB, although it appears that TSEB-A has a slightly greater bias in soil temperatures (Tables 2 and 3; Figs. 2 and 3). The soil temperatures from TSEB generally have greater deviations from the observations particularly on DOY 192 and 195. However, it is also important to point out that canopy cover/LAI was high for these two days (see Table 1 and discussion below) making it difficult to derive a soil temperature using TSEB with the composite temperature.

The TSEB-A model produces smaller RMSE values compared to TSEB. Results from TSEB and TSEB-A are similar in the early and late growing season. However, there is a poorer agreement between the TSEB-derived soil temperatures and the observations during mid-season (DOY 192 and 195) when significant advection resulting in small land surface-air temperature differences and extremely small and sometimes negative *H* values in the afternoons. The LAI was ~4.5, and the fractional vegetation cover reached 0.95. This caused large uncertainty in the estimation of soil temperature from the composite radiometric temperature since the solution is obtained by dividing by $1 - f_c(\theta) \sim 0.05$ (see Eq. (7)). For the selected days, the discrepancy between modeled and measured soil temperature ranges from 2.54 to −17.06 K, with mean value of −6.21 K for DOY 192 and 195. These errors could introduce large errors in *E* and *T* estimation using the TSEB model.

The performance of the TSEB and TSEB-A model output of the fluxes were evaluated using measurements from the EC system on the three days where TSEB derived component temperatures had the largest disagreement with the observations, namely for

Table 3
Statistical results of modeled vs. measured energy and mass flux variables at the HiWATER site.

		Rn (W/m^2)	G_0 (W/m^2)	*H* (W/m^2)	*LE* (W/m^2)	*ET* (mm/d)
Measured	Mean	392	38	22	332	4.6
	SD	204	35	40	167	1.4
TSEB-A	Mean	395	43	8	343	4.8
	SD	202	27	11	187	1.5
	MBE	4	6	−15	12	0.2
	MAPD	2%	53%	86%	10%	6.6%
	RMSE	16	26	35	50	0.4
TSEB	Mean	370	45	22	289	4.0
	SD	209	35	37	171	1.5
	MBE	−27	7	13	−41	−0.6
	MAPD	6%	52%	96%	14%	13%
	RMSE	28	28	33	59	0.7

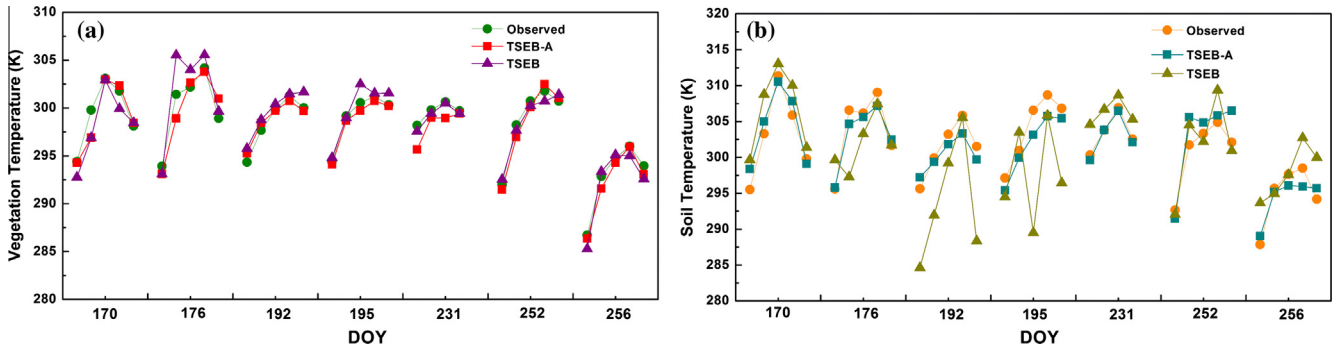

Fig. 2. Measured versus modeled vegetation (a), and soil (b) temperatures using TSEB-A model and TSEB model.

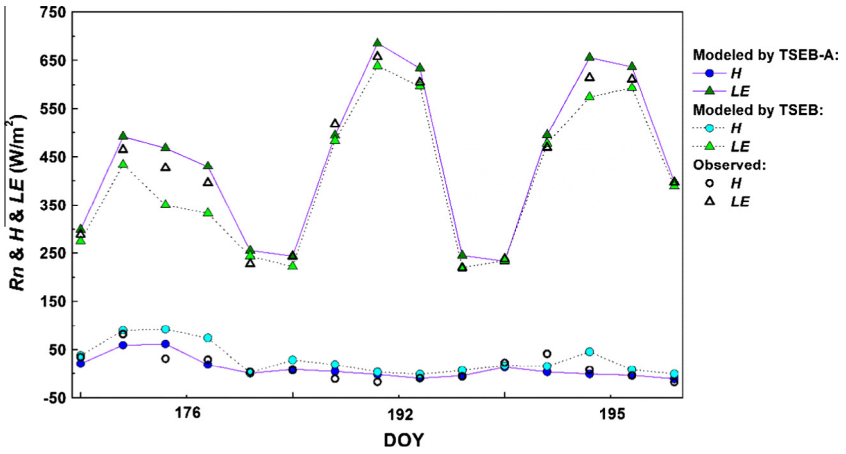

Fig. 3. Daytime fluxes measured in HiWATER compare to modeled daytime fluxes from the TSEB-A and TSEB models on DOY 176, 192 and 195.

DOY 176, 192, 195. The 2 h interval time series of TSEB and TSEB-A models output of fluxes are shown in Fig. 3. For TSEB, although there are significant differences between modeled and measured soil component temperature, there is good agreement between modeled output from both TSEB and TSEB-A, and observed surface energy fluxes on these days. For TSEB on DOY 192 and 195, the relatively small differences between modeled and observed vegetation temperatures but large differences between modeled and observed soil temperatures, did not affect the total *ET* flux since vegetation cover was high. Although there may be good results in the total *LE* or *ET* using either model, the partitioning between soil and vegetation *LE* or *E* and *T*, respectively, may not be as reliable, particularly for TSEB.

4.2. TSEB-A model performance against EC flux measurements over the whole growing season

The TSEB-A and TSEB models were evaluated using half hourly flux measurements of *Rn*, G_0, *LE*, *H* from HiWATER and *Rn*, G_0 and *LE* from BEAXRE08 (Figs. 4 and 5 and Tables 3 and 4). The agreement between measured and estimated fluxes from the both models are reasonable over the entire growing season in the two study areas, but slightly better results were obtained with the TSEB-A model.

The TSEB-A model generally underestimates *H* for the HiWATER site, particularly when the measurements exceed 50 W m^{-2}, showing a significant bias, but considerably less scatter compared to TSEB. Yet, there is overall better agreement with the *LE* flux observations using TSEB-A, which is due in part to generally small *H* values observed during most of the growing season. As a result, the mean absolute percent deviation (MAPD) value for *H* is over 85% and is due in part to many extremely low values in *H* at HiWATER, including negative values from the irrigated maize crop which often occurred during mid-season with high vegetation biomass and strong advection (see Fig. 4). However, it is also likely that the significant underestimates in *H* when measured values were ~100 W m^{-2} is due to the overestimate of soil evaporation under these conditions (see discussion regarding (Fig 9)).

There is also a similar error but significant discrepancy between TSEB-A modeled and measured G_0 for both sites, with the MAPD being 50% for both the HiWATER and BEAREX08 field sites. This is due in part to the relatively small magnitude and range in the observed values from the two sites combined with the simplicity of the approach in estimating G_0. Nevertheless, the relatively large MAPD values for *H* or G_0 in these two sites do not adversely affect the performance of the model for estimating *LE*.

The TSEB-A model produced *LE* with MAPD of 10% versus 14% from TSEB model for HiWATER, which both are less than the uncertainty of the EC measurements (i.e. estimated to be approximately 15% for HiWATER; see Wang et al. (2015). TSEB-A and TSEB models produced slightly greater MAPD values of 20% and 34%, respectively. The larger MAPD values for the BEAREX08 site is caused to some extent by the fact that during certain periods during the growing season, the lysimeter ET was not representative of the surrounding field ET due to difference in the amount of crop cover inside and outside the lysimeter (Kustas et al., 2015). The larger discrepancies for *LE* estimated from TSEB model with the BEAREX08 data is likely due in part to the greater scatter between measured and modeled *Rn* which is related to the differences in the temperature partitioning algorithm used by TSEB-A versus TSEB.

The fluctuations of measured and TSEB-A estimated daytime (9:00–18:00 for HiWATER and 8:00–18:00 for BEAREX08, local time) *ET* and its components are illustrated in Fig. 6 and scatter

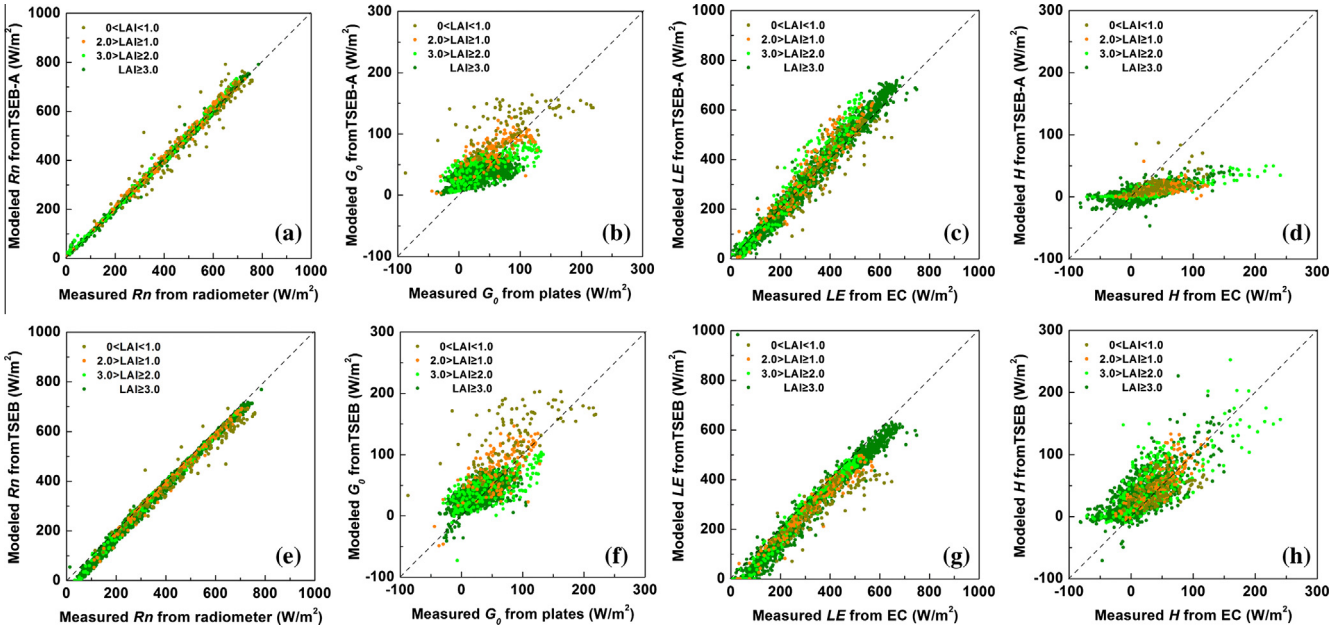

Fig. 4. Scatter plots of the comparison of the energy components derived from the TSEB-A and TSEB model with the measurements from HiWATER, TSEB-A: (a) *Rn*; (b) G_0; (c) *LE* and (d) *H*; TSEB: (e) *Rn*; (f) G_0; (g) *LE* and (h) *H*.

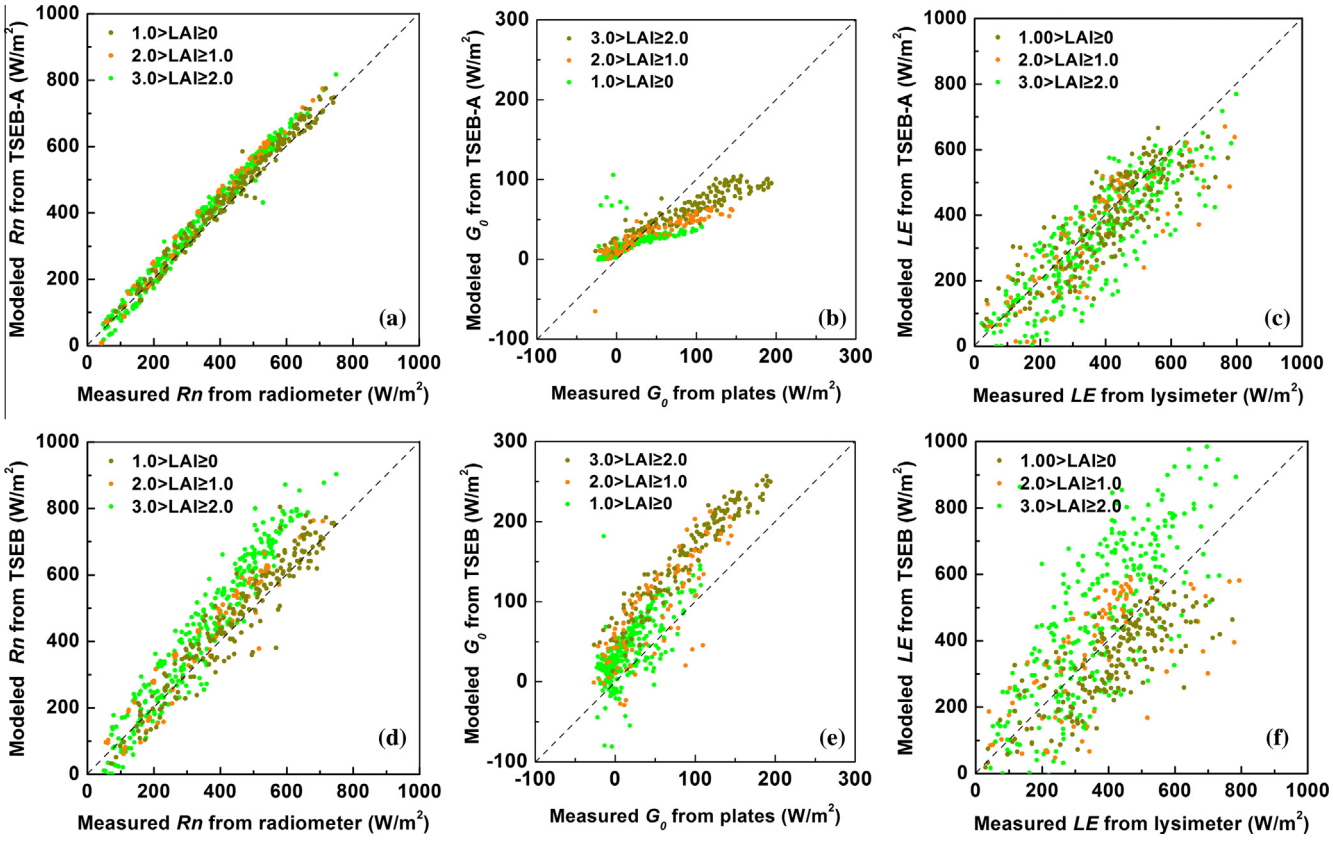

Fig. 5. Scatter plots of the comparison of the energy components derived from the TSEB-A and TSEB model with the measurements from BEAREX08, TSEB-A: (a) *Rn*; (b) G_0 and (c) *LE*; TSEB: (d) *Rn*; (e) G_0 and (f) *LE*.

plot in Fig. 7. The observed and modeled *LE* fluxes and the components fluxes from soil and canopy are converted to units of mass flux (mm/d) to coincide with the customary unit used in agricultural water management applications. In this case, a good agreement between measured and estimated daytime *ET* was obtained with values of bias, RMSE and MAPD equal to 0.17 mm, 0.39 mm and 7% for HiWATER and −0.12 mm, 0.42 mm and 10% for the BEAREX08, which are comparable to the accuracy typically required for field water management (see e.g., Seguin et al. (1999)) (Fig. 7).

Table 4
Statistical results of modeled vs. measured energy and mass flux variables at the BEAREX08 site.

		Rn (W/m^2)	G_0 (W/m^2)	LE (W/m^2)	ET (mm/d)
Measured	Mean	381	47	382	5.5
	SD	174	53	165	1.3
TSEB-A	Mean	414	34	347	5.3
	SD	186	30	161	0.9
	MBE	29	−13	−33	−0.2
	MAPD	9%	52%	20%	10%
	RMSE	40	35	95	0.4
TSEB	Mean	370	45	289	6.2
	SD	209	35	171	1.6
	MBE	54	39	21	0.7
	MAPD	19%	94%	34%	23%
	RMSE	91	50	166	2.3

The modeled *ET*, *E* and *T* over the course of a season provides detailed behavior of the soil and plant water use and crop growth dynamics at different periods affected by different environmental conditions. There is significant oscillation in daytime *ET* mainly due to the variations during the early season in *E* and then in *T* (see Fig. 6c and d). This was due in part to temporal variations in water availability (mainly the near surface moisture affecting *E*), but the amount of radiation (cloudiness) and increase in LAI were also significant factors affecting *T*. In HiWATER both modeled and observed *ET* reach a maximum of 6 mm prior to DOY 180 when LAI was <3.5, while the maximum of 8 mm was observed during the period DOY 180 to DOY 230 when LAI ranged between 3 and 4.5. After DOY 230 as the corn started to go through senescence, maximum *ET* was again around 6 mm. For BEAREX08, the observed maximum *ET* with values above 8 mm was around DOY 215 when the LAI reached peaked at about 3.0, while the modeled values higher than 7 mm were computed. After attaining the 7–8 mm *ET* plateau, the daytime *ET* gradually declined as the cotton began to go through senescence and consequently the canopy transpiration rate decreased.

As mentioned earlier, the seasonal variation in modeled *T* was significantly larger than *E* for much of the growing season (Fig. 6c and d). In the HiWATER *prior* to DOY 180, the crops grew rapidly, with the field estimated LAI increasing from 0.4 to 3.2, but the cotton grew gradually prior to DOY210 in BEAREX08 and the LAI increased from nearly 0 to 1.8. This resulted in a substantial decrease in radiation and wind speed near the soil surface, both contributing to a decrease in *E*. During these periods of peak LAI, which was from DOY 188 to 218 in HiWATER and from DOY 218 to 238 in BEARXE08, *T* was relatively high at more than 5 mm, while *E* from the soil remained low and fairly constant with only small fluctuations due to rainfall and irrigation events. After DOY 230 in HiWATER and DOY 240 in BEAREX08, *T* from TSEB-A began to gradually decrease, with values converging towards soil *E*; this is attributed to crop senescence resulting in a gradual decrease in green vegetation fraction and LAI, which resulted in greater radiation and wind speed at the soil surface. In addition, there are notable discrepancies between the modeled and observed *ET* in HiWATER at the very end of the season when the maize went through rapid senescence. During this period, the estimated green vegetation fraction as derived from the imagery did not capture this decrease, which greatly affected the performance of the TSEB-A model. However, in the BEAREX08, the TSEB-A model seemed to reliably tracked the gradual decline in green fraction of cotton canopy.

4.3. TSEB model performance partitioning ET to T and E

An initial evaluation of TSEB and TSEB-A model performance in partitioning the latent heat flux, output for the same three days, DOY 176, 192 and 195 having component temperatures. The ratios of *T*/*ET* estimated by TSEB were 69%, 76% and 88%, at 13:00 local time on these days, respectively, whereas the observed values were 89%, 87% and 80%, respectively. The TSEB-A model estimated a *T*/*ET* ratio of 82%, 87% and 88%, respectively. For DOY 176 and 192 TSEB computed a lower *T* than observed suggesting TSEB overestimated E/ET given that the total *LE* is in good agreement with the

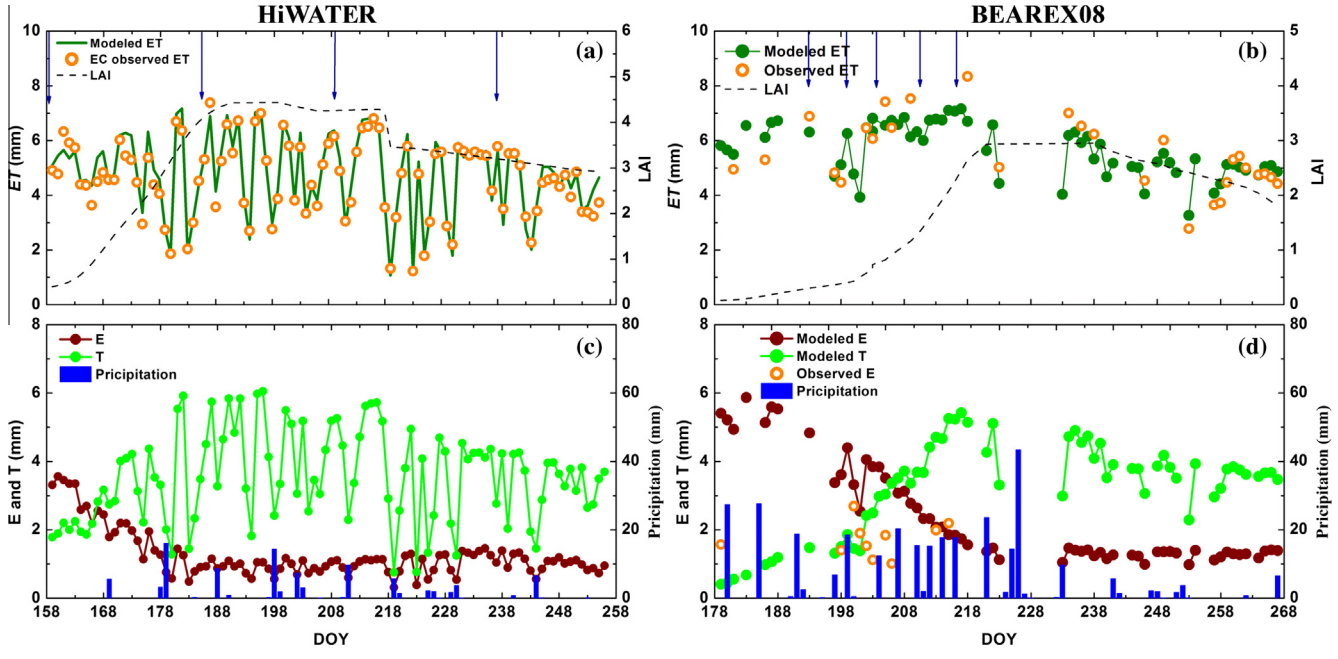

Fig. 6. Seasonal variation in modeled daytime (9:00–18:00 for HiWATER and 8:00–18:00 for BEAREX08, local time) *ET* by TSEB-A (mm day^{-1}) (a and b) *E* and *T* (c and d) compared with measurements from the EC system in HiWATER and from lysimeter and microlysimeters in BEAREX08 site. The blue arrows represent irrigations during the season.

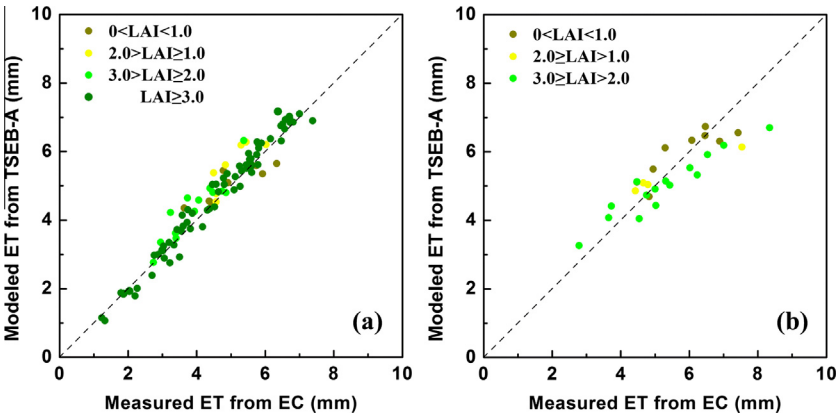

Fig. 7. Scatter plots of the comparison of the *ET* derived from the TSEB-A and measurements from the EC system in (a) HiWATER and from lysimeter and microlysimeters in (b) BEAREX08 site.

measurements from the EC system (Fig. 3). The MB values between TSEB-derived *T* and *E* and values estimated from the *EC* system and stable oxygen and hydrogen isotope technology yielded values of −96 and 57 W/m^2 for *T* and *E*, respectively. The application of TSEB-A provided more accurate partitioning of *T* and *E* than TSEB resulting in bias between modeled and observed for *T* and *E* of 7 and 24 W/m^2, and less discrepancy with observations. This comparison suggests that the TSEB-A model can provide not only reliable *ET* values but also reasonable estimates of the partitioning between *T* and *E* under these conditions. This conclusion, however, comes with the caveat that the α_c and α_s value needs to be reliably estimated or determined *a priori* for the TSEB-A formulations (Eqs. (6) and (9)) to compute robust canopy and soil temperatures and the requirement of surface soil moisture observations, which are not routinely available at field scale.

For HiWATER a more extensive evaluation of TSEB-A model *T* and *E* partitioning was conducted using ratios of *E*/*ET* and *T*/*ET* estimated from isotope technology (Williams et al., 2004). The TSEB-A model yielded similar estimates of *E*/*ET* and *T*/*ET* with those derived from isotope approach in this study for the midday period (13:00–15:00 LST) for the entire growing season (Figs. 8 and 9). There is a fair level of scatter with a MAPD value of 27% and 11% for *E*/*ET* and *T*/*ET*, respectively and greater discrepancy occurred between modeled and measured under partial vegetation cover

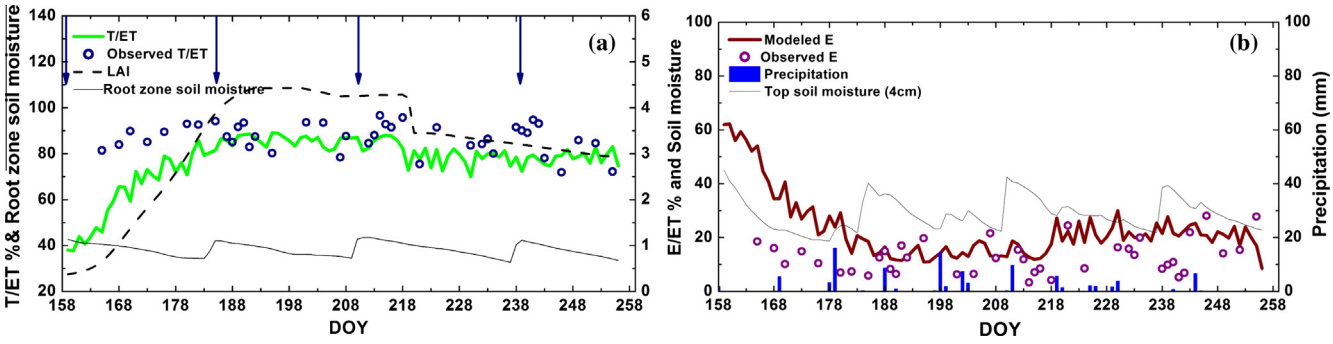

Fig. 8. Comparison of the modeled (a) *T*/*ET*% and (b) *E*/*ET*% values from the TSEB-A model with the ground-based measurement data using the stable oxygen and hydrogen isotope technique for HiWATER field site. Soil moisture values represent the top 4 cm and the root zone soil moisture values are averaged from 40 cm and 80 cm depths in the soil profile. The arrows are the field irrigation times.

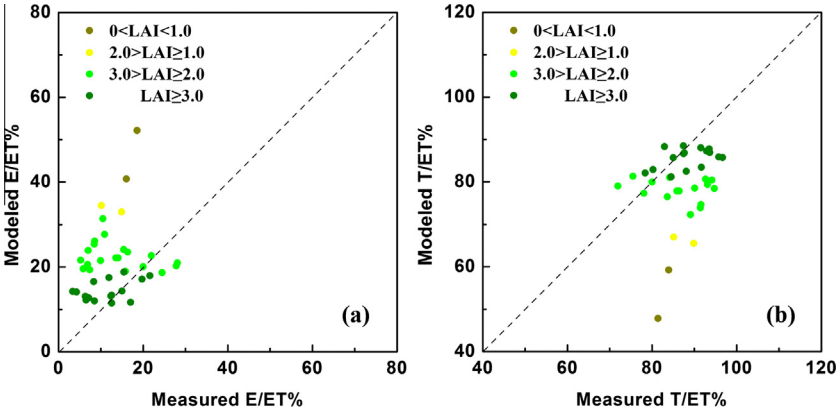

Fig. 9. Scatter plots of the comparison of the (a) *E*/*ET*% and (b) *T*/*ET* derived from the TSEB-A model with the measurements from HiWATER.

conditions generally leading to an overestimate of E and underestimate of T (Fig. 9). Moreover the data are mainly from the two extremes of high/low E/ET and T/ET. The seasonal trends in E/ET and T/ET over the maize site given by the TSEB-A model follow the temporal trend in LAI, with rapid increase (decrease) in T/ET (E/ET) followed by a plateau in these values and then a gradual decrease (increase) in T/ET (E/ET) as the crop LAI decreases due to senescence. Day-to-day variations in both modeled and observed E/ET and T/ET varied due to oscillations in solar radiation forcing and atmospheric demand (vapor pressure, air temperature and wind speed) (Williams et al., 2004), and the impact of the rainfall, and irrigation events.

In the early season (before DOY 180), more than 40% of the water use via soil evaporation did not contribute to crop growth and development. The E/ET decreased gradually as the fraction of green vegetation/LAI increased and the surface soil began to dry (Fig. 8a). By mid-season, the E/ET and T/ET values appeared to plateau to about 15% and 85%, respectively, even though there were periodic irrigations and the rainfall events. This is likely due to the fact that the field is nearly complete canopy cover with little radiation reaching the soil surface and most wind attenuated by the canopy affecting E rates. Later in the season as the crop began to undergo senescence resulting in decreasing canopy cover and transpiration rate whereas the field was still irrigated with a few rainfall events. As a result E/ET increased with values for some days being greater than 20% due to high surface soil water content and a more open canopy. Both the measurements and model output of E and T indicate that improvements in water use efficiency in advective environments will be most effective early and later in the growing season where there is abundant water lost from wet surface soil conditions that are not contributing to crop growth and development. This requires irrigation applications that minimize replenishing top surface moisture and also versus root zone moisture using irrigation techniques such as drip irrigation system as opposed to flood irrigation practices (Er-Raki et al., 2010).

For the BEAREX08, the modeled E were compared with measurements from two replicates of five microlysimeters each that were deployed along a cross section of the interrow diagonally. The TSEB-A model overestimated E resulted in bias and RMSE of 1.3 and 1.7 mm over the growing season. However, the overestimation only appeared during the early season when there was low vegetation cover but with wet soil conditions; there were small discrepancies with the E measurements during the mid-season (DOY 213, 215). During the early season (DOY < 200), more than 80% of the daytime ET was contributed by E for the BEAREX08 site, which is consistent with the results from Sánchez et al. (2015) indicating that daytime E is the main contribution to daytime ET when vegetation cover fractions is below 0.2.

In BEAREX08, the modeled daytime E was higher than 5 mm in the early season, and then declined gradually, but the T increased gradually as the cotton grew rapidly (Fig. 6d). The soil E values appeared to plateau at about 2 mm after the field LAI approached maximum and turned out to be a slight increase, but T has fluctuations as the solar radiation varied and declined gradually as the crop began to go through senescence.

5. Discussion

The model evaluation using half hourly flux measurements showed that there were relatively large discrepancies between modeled and observed H and G_0 (large MAPD values), as already noted, but this did not lead to a large uncertainty in LE estimation (MAPD = 10% and 20% for HiWATER and BEAREX08, respectively) due to the relatively small contribution of these two terms to the surface energy balance (measured H/Rn and G_0/Rn are 6% and 10%, respectively) (see Table 3) under strongly advective irrigated and dense vegetation covered conditions. Besides errors in estimating f_G, the errors in modeled H are due also in part to underestimation in composite temperature from the longwave radiometer since the sensor mainly viewed the top and greener portion of the maize which was likely cooler than the integrated composite temperature of the whole canopy plant containing senescent leaves, particularly towards the end of the season (Morillas et al., 2013). For example, in HiWATER, there is a ~2.0 K lower composite temperature from the temperature measurements using the longwave radiometer later in the season (Fig. 1) compared with T_{rad} derived from the thermal infrared camera, which viewed the whole maize canopy as well as soil temperatures from the angular observation. Therefore, the underestimated composite temperature resulted in the underestimation of H, finally causing the overestimated LE (e.g., DOY 252–256) for HiWATER.

A slight discrepancy was found between the E/ET or T/ET estimated from the TSEB-A model and measured from HiATER. While neglecting the uncertainties of the TSEB-A model, however, investigations also indicated that δ_{ET} measured with flux-gradient method can introduce uncertainty of nearly 5‰ from rain and irrigation events, which produces a ten-fold increase in the uncertainty in T/ET observations (Huang and Wen, 2014). For example, the E/ET value decreases to near zero between DOY 209 and 219, which does not seem physically plausible for a wet soil from recent irrigation and precipitation events (see Fig. 8). For the BEAREX08, there were larger discrepancies between the E estimated from the TSEB-A model and measured from microlysimeters. These larger discrepancies during early season might be related to local spatial differences in soil water content and plant cover between the large weighing lysimeter and the area surrounding the microlysismetrs, in addition to inconsistencies between the model assumptions in the early season. For instance, during the early growing season, the soil surface may not be uniformly wet so the estimated α_s value of 1.2, may have been too high resulting in an overestimation of E.

The TSEB-A model has been successfully applied to estimate the E, T and the total ET during the entire growing season in arid environments in the US and China containing irrigated agriculture. As described earlier, the TSEB-A model requires the acquisition of accurate α_s and α_c parameters, which may limit its application for operational purposes unless it can be estimated under complex environment conditions.

To assess the reliability of the model derived ET, E/ET and T/ET, an uncertainty analysis method proposed by Marx et al. (2008) was used. For TSEB-A, the Priestley-Taylor coefficients for soil, α_s, and vegetation, α_c, are crucial parameters in the proposed formulations, so the possible uncertainty introduced by these parameters was analyzed. In the first step, ET, E and T were calculated using the α_s and α_c value derived from the method introduced in Section 2 and then these outputs were re-computed by using an uncertainty bound of ±20% α_s and α_c and shown in Fig. 10.

The ET computed by TSEB-A with the ±20% uncertainty in α_s and α_c values yield the greatest variability during the early season when fields have low plant cover vegetated and late in the season when the plants are undergoing senescence (Fig. 10). This happens to be associated with the condition of low vegetation fraction in the early season and low green vegetation fraction in the later season which affects the energy partitioning between soil and vegetation (Fig. 10c and d). These are also periods where there will be large variations in the partitioning of ET into E and T, mainly after rainfall and irrigation events during the mid-season in combination with high atmospheric demand with high net radiation and hot, dry, but breezy conditions (strong advection).

The TSEB-A model requires soil moisture as *a priori* information to estimate soil temperature, however, the soil moisture derived

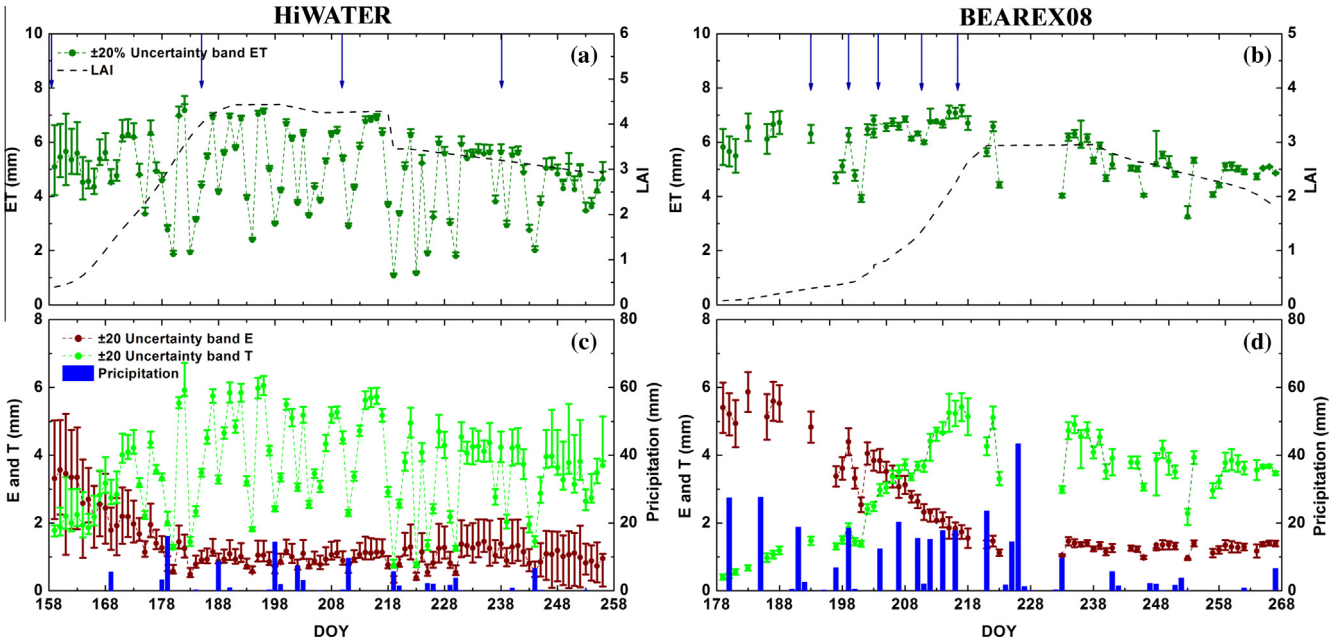

Fig. 10. Sensitivity analysis by deviating α_s and setting α_c with ±20% uncertainty band over the whole growing season with irrigations events illustrated as blue arrows. (a and b) variation of daytime modeled *ET* in HiWATER and BEARXE08 sites; (c and d) variation of daytime modeled *E*, *T* in HiWATER and BEARXE08.

uncertainty should be considered if the model is applied combining with remote sensing supplied thermal infrared date. Fortunately, error test results showed that the uncertainty of soil moisture estimation would introduce less than 20% on α_s adjustment, where the soil moisture value ranges from 0.1 to 0.3 with uncertainties from 0% to 30%. According to the TSEB-A model sensitivity analysis, the soil moisture estimation uncertainty may lead to errors (MAPD values) of around 5% in *ET* and *T* and *E*.

6. Summary and conclusions

Evaluation of the original TSEB versus the proposed TSEB-A model indicates that the TSEB approach is more likely to produce greater errors in estimating soil and vegetation component temperatures and *E* and *T*, particularly under high vegetation cover, which may be exacerbated under advective conditions. The TSEB-A was not as sensitive to these conditions, which was attributed to a modified approach to partition soil and canopy temperature from radiometric temperature, producing robust estimates of daytime *ET*, with a MAPD of 10% in HiWATER in China and of 20% in BEAREX08 in the U.S. In addition, the ratios *of E*/*ET* and *T*/*ET* and *E* estimated using TSEB-A model is in reasonable agreement with values computed using the stable isotopic method and EC technique in HiWATER over a growing season and measured from microlysimeters in BEARXE08 in the early growing season. However, the TSEB-A approach requires defining two key variables α_s and α_c which still do not account for VPD variation and heterogeneous vegetation conditions. In addition, estimates of surface soil moisture are needed, which may be available from *in-situ* measurements in conjunction with disaggregated microwave satellite soil moisture products (Merlin et al., 2013). A sensitivity analysis suggests that using α_s and α_c with ±20% uncertainty over the entire growing season can lead to errors (MAPD values) of around 5% in *ET* and *T* and *E*, but larger in the early growing season and later in the season when crops undergo senescence under partial vegetation cover conditions.

Future studies should address how to estimate nominal α_s and α_c values *a priori* when applying the TSEB-A model and resulting error/uncertainty under the different landscapes and environment conditions. This could involve *in-situ* measurements and microwave remote sensing estimates of surface soil water that could be used to define or constrain the value of α_s (Kustas et al., 2003), to extend application of TSEB-A model to large scales. Although satellite-based microwave sensors currently cannot provide soil moisture estimates at field scale. More studies over landscapes having limited irrigation production or natural dryland systems where water stress would be more prevalent are needed that include a long time series of composite radiometric temperatures, soil and vegetation component temperatures, surface soil moisture in addition to estimates of *E* and *T*.

Acknowledgments

We thank all the scientists, engineers, and students who participated in HiWATER and BEARXE08 field campaigns. This work was supported by the National Basic Research Program of China (2015CB953702) and National Natural Science Foundation of China (41531174). We would like to thank Professor Xuefa Wen at Synthesis Research Center of China Ecosystem Research Network, Key Laboratory of Ecosystem Network Observation and Modeling, Institute of Geographic Science and Natural Resource, Chinese Academy of Science, Beijing China. The authors also especially would like to thank Professor Guoyu Qiu at School of Environment and Energy, Shengzhen Graduate School of Peking University for thermal images collected from the thermal camera. Thanks to two anonymous reviewers for their valuable comments and suggestions on our manuscript. BEAREX08 was supported by the USDA-ARS National Program 211, Water Availability and Watershed Management and in part by the Ogallala Aquifer Program, a consortium between USDA-Agricultural Research Service, Kansas State University, Texas AgriLife Research, Texas AgriLife Extension Service, Texas Tech University, and West Texas A&M University. USDA is an equal opportunity employer and provider.

References

Agam, N., Evett, S.R., Tolk, J.A., Kustas, W.P., Colaizzi, P.D., Alfieri, J.G., McKee, L.G., Copeland, K.S., Howell, T.A., Chávez, J.L., 2012. Evaporative loss from irrigated

interrows in a highly advective semi-arid agricultural area. Adv. Water Resour. 50, 20–30.
Agam, N., Kustas, W.P., Anderson, M.C., Norman, J.M., Colaizzi, P.D., Howell, T.A., Prueger, J.H., Meyers, T.P., Wilson, T.B., 2010. Application of the Priestley–Taylor approach in a two-source surface energy balance model. J. Hydrometeorol. 11, 185–198.
Alfieri, J.G., Kustas, W.P., Prueger, J.H., Hipps, L.E., Evett, S.R., Basara, J.B., Neale, C.M. U., French, A.N., Colaizzi, P., Agam, N., Cosh, M.H., Chavez, J.L., Howell, T.A., 2012. On the discrepancy between eddy covariance and lysimetry-based surface flux measurements under strongly advective conditions. Adv. Water Resour. 50, 62–78.
Anderson, M.C., Norman, J.M., Kustas, W.P., Li, F., Prueger, J.H., Mecikalski, J.R., 2005. Effects of vegetation clumping on two-source model estimates of surface energy fluxes from an agricultural landscape during SMACEX. J. Hydrometeorol. 6, 892–909.
Anderson, M.C., Kustas, W.P., Norman, J.M., Hain, C.R., Mecikalski, J.R., Schultz, L., González-Dugo, M.P., Cammalleri, C., d'Urso, G., Pimstein, A., Gao, F., 2011. Mapping daily evapotranspiration at field to continental scales using geostationary and polar orbiting satellite imagery. Hydrol. Earth Syst. Sci. 15, 223–239.
Anderson, M.C., Kustas, W.P., Alfieri, J.G., Gao, F., Hain, C., Prueger, J.H., Evett, S., Colaizzi, P., Howell, T., Chávez, J.L., 2012. Mapping daily evapotranspiration at landsat spatial scales during the BEAREX'08 field campaign. Adv. Water Resour. 50, 162–177.
Campbell, G.S., Norman, J.M., 1998. An Introduction to Environmental Biophysics, vol. 286. Springer, New York.
Colaizzi, P.D., Kustas, W.P., Anderson, M.C., Agam, N., Tolk, J.A., Evett, S.R., Howell, T. A., Gowda, P.H., O'Shaughnessy, S.A., 2012a. Two-source energy balance model estimates of evapotranspiration using component and composite surface temperatures. Adv. Water Resour. 50, 134–151.
Colaizzi, P.D., Schwartz, R.C., Evett, S.R., Howell, T.A., Gowda, P.H., Tolk, J.A., 2012b. Radiation model for row crops: II. Model evaluation. Agron. J. 104, 241–255.
Colaizzi, P.D., Agam, N., Tolk, J.A., Evett, S.R., Howell, T.A., Gowda, P.H., O'Shaughnessy, S.A., Kustas, W.P., Anderson, M.C., 2014. Two-source energy balance model to calculate E, T, and ET: comparison of Priestley–Taylor and Penman–Monteith formulations and two time scaling methods. Trans. ASABE 57, 479–498.
Donohue, R.J., Roderick, M.L., McVicar, T.R., 2008. Deriving consistent long-term vegetation information from AVHRR reflectance data using a cover-triangle-based framework. Remote Sens. Environ. 112, 2938–2949.
Er-Raki, S., Chehbouni, A., Boulet, G., Williams, D.G., 2010. Using the dual approach of FAO-56 for partitioning ET into soil and plant components for olive orchards in a semi-arid region. Agric. Water Manage. 97, 1769–1778.
Evett, S.R., Agam, N., Kustas, W.P., Colaizzi, P.D., Schwartz, R.C., 2012a. Soil profile method for soil thermal diffusivity, conductivity and heat flux: comparison to soil heat flux plates. Adv. Water Resour. 50, 41–54.
Evett, S.R., Kustas, W.P., Gowda, P.H., Anderson, M.C., Prueger, J.H., Howell, T.A., 2012b. Overview of the Bushland Evapotranspiration and Agricultural Remote sensing EXperiment 2008 (BEAREX08): a field experiment evaluating methods for quantifying ET at multiple scales. Adv. Water Resour. 50, 4–19.
Evett, S.R., Schwartz, R.C., Howell, T.A., Baumhardt, R. Louis, Copeland, K.S., 2012c. Can weighing lysimeter ET represent surrounding field ET well enough to test flux station measurements of daily and sub-daily ET? Adv. Water Resour. 50, 79–90.
Fisher, J.B., Tu, K.P., Baldocchi, D.D., 2008. Global estimates of the land–atmosphere water flux based on monthly AVHRR and ISLSCP-II data, validated at 16 FLUXNET sites. Remote Sens. Environ. 112, 901–919.
Good, S.P., Noone, D., Bowen, G., 2015. Hydrologic connectivity constrains partitioning of global terrestrial water fluxes. Science 349, 175–177.
Guzinski, R., Anderson, M.C., Kustas, W.P., Nieto, H., Sandholt, I., 2013. Using a thermal-based two source energy balance model with time-differencing to estimate surface energy fluxes with day-night MODIS observations. Hydrol. Earth Syst. Sci. Discuss. 10, 1897–1941.
Hu, Z., Wen, X., Sun, X., Li, L., Yu, G., Lee, X., Li, S., 2014. Partitioning of evapotranspiration through oxygen isotopic measurements of water pools and fluxes in a temperate grassland. J. Geophys. Res.: Biogeosci. 119, 2013JG002367.
Huang, L., Wen, X., 2014. Temporal variations of atmospheric water vapor δD and $\delta^{18}O$ above an arid artificial oasis cropland in the Heihe River Basin. J. Geophys. Res.: Atmos. 10, 2014JD021891.
Jasechko, S., Sharp, Z.D., Gibson, J.J., Birks, S.J., Yi, Y., Fawcett, P.J., 2013. Terrestrial water fluxes dominated by transpiration. Nature 496, 347–350.
Kool, D., Agam, N., Lazarovitch, N., Heitman, J.L., Sauer, T.J., Ben-Gal, A., 2014. A review of approaches for evapotranspiration partitioning. Agric. For. Meteorol. 184, 56–70.
Kustas, W.P., Norman, J.M., 1999. Evaluation of soil and vegetation heat flux predictions using a simple two-source model with radiometric temperatures for partial canopy cover. Agric. For. Meteorol. 94, 13–29.
Kustas, W.P., Bindlish, R., French, A.N., Schmugge, T.J., 2003. Comparison of energy balance modeling schemes using microwave-derived soil moisture and radiometric surface temperature. Water Resour. Res. 39, 1039.
Kustas, W., Anderson, M., 2009. Advances in thermal infrared remote sensing for land surface modeling. Agric. For. Meteorol. 149, 2071–2081.
Kustas, W.P., Alfieri, J.G., Anderson, M.C., Colaizzi, P.D., Prueger, J.H., Evett, S.R., Neale, C.M.U., French, A.N., Hipps, L.E., Chávez, J.L., Copeland, K.S., Howell, T.A., 2012. Evaluating the two-source energy balance model using local thermal and surface flux observations in a strongly advective irrigated agricultural area. Adv. Water Resour. 50, 120–133.
Kustas, W., Alfieri, J., Evett, S., Agam, N., 2015. Quantifying variability in field-scale evapotranspiration measurements in an irrigated agricultural region under advection. Irrig. Sci. 33, 325–338.
Lee, X., Kim, K., Smith, R., 2007. Temporal variations of the $^{18}O/^{16}O$ signal of the whole-canopy transpiration in a temperate forest. Glob. Biogeochem. Cycl. 21, GB3013.
Li, F., Kustas, W.P., Prueger, J.H., Neale, C.M.U., Jackson, T.J., 2005. Utility of remote sensing-based two-source energy balance model under low- and high-vegetation cover conditions. J. Hydrometeorol. 6, 878–891.
Li, F., Kustas, W.P., Anderson, M.C., Jackson, T.J., Bindlish, R., Prueger, J.H., 2006. Comparing the utility of microwave and thermal remote-sensing constraints in two-source energy balance modeling over an agricultural landscape. Remote Sens. Environ. 101, 315–328.
Li, H., Sun, D., Yu, Y., Wang, H., Liu, Y., Liu, Q., Du, Y., Wang, H., Cao, B., 2014. Evaluation of the VIIRS and MODIS LST products in an arid area of Northwest China. Remote Sens. Environ. 142, 111–121.
Li, X., Cheng, G., Liu, S., Xiao, Q., Ma, M., Jin, R., Che, T., Liu, Q., Wang, W., Qi, Y., Wen, J., Li, H., Zhu, G., Guo, J., Ran, Y., Wang, S., Zhu, Z., Zhou, J., Hu, X., Xu, Z., 2013. Heihe watershed allied telemetry experimental research (HiWATER): scientific objectives and experimental design. Bull. Am. Meteorol. Soc. 94, 1145–1160.
Liebethal, C., Huwe, B., Foken, T., 2005. Sensitivity analysis for two ground heat flux calculation approaches. Agric. For. Meteorol. 132, 253–262.
Liu, S., Xu, Z., Wang, W., Jia, Z., Zhu, M., Bai, J., Wang, J., 2011. A comparison of eddy-covariance and large aperture scintillometer measurements with respect to the energy balance closure problem. Hydrol. Earth Syst. Sci. 15, 1291–1306.
Liu, S., Xu, Z., Zhu, Z., Jia, Z., Zhu, M., 2013. Measurements of evapotranspiration from eddy-covariance systems and large aperture scintillometers in the Hai River Basin, China. J. Hydrol. 487, 24–38.
Liu, S., Xu, Z., Song, L., Zhao, Q., Xu, T., Ge, Y., Ma, Y., Zhu, Z., Jia, Z., Zhang, F., 2016. Upscaling evapotranspiration measurements from multi-site to the satellite pixel scale over heterogeneous land surfaces. Agric. For. Meteorol. http://dx.doi.org/10.1016/j.agrformet.2016.04.008.
Long, D., Singh, V.P., 2012. A two-source trapezoid model for evapotranspiration (TTME) from satellite imagery. Remote Sens. Environ. 121, 370–388.
Marek, T.H., Schneider, A.D., Howell, T.A., Ebeling, L.L., 1988. Design and construction of large weighing monolithic lysimeters. Trans. ASABE. 31, 477–484.
Marx, A., Kunstmann, H., Schüttemeyer, D., Moene, A.F., 2008. Uncertainty analysis for satellite derived sensible heat fluxes and scintillometer measurements over Savannah environment and comparison to mesoscale meteorological simulation results. Agric. For. Meteorol. 148, 656–667.
McVicar, T.R., Van Niel, T.G., Li, L., Hutchinson, M.F., Mu, X., Liu, Z., 2007. Spatially distributing monthly reference evapotranspiration and pan evaporation considering topographic influences. J. Hydrol. 338, 196–220.
Merlin, O., Escorihuela, M.J., Mayoral, M.A., Hagolle, O., Al Bitar, A., Kerr, Y., 2013. Self-calibrated evaporation-based disaggregation of SMOS soil moisture: an evaluation study at 3 km and 100 m resolution in Catalunya, Spain. Remote Sens. Environ. 130, 25–38.
Morillas, L., García, M., Nieto, H., Villagarcia, L., Sandholt, I., Gonzalez-Dugo, M.P., Zarco-Tejada, P.J., Domingo, F., 2013. Using radiometric surface temperature for surface energy flux estimation in mediterranean drylands from a two-source perspective. Remote Sens. Environ. 136, 234–246.
Mu, X., Hu, R., Huang, S., Chen, Y., 2013. HiWATER: Dataset of Emissivity in the Middle Reaches of the Heihe River Basin in 2012. Heihe Plan Science Data Center.
Norman, J.M., Kustas, W.P., Humes, K.S., 1995. Two source approach for estimating soil and vegetation energy fluxes in observations of directional radiometric surface temperature. Agric. For. Meteorol. 77, 263–293.
Priestley, C.H.B., Taylor, R.J., 1972. On the assessment of surface heat flux and evaporation using large-scale parameters. Mon. Weather Rev. 100, 81–92.
Richardson, A.D., Hollinger, D.Y., Burba, G.G., Davis, K.J., Flanagan, L.B., Katul, G.G., William Munger, J., Ricciuto, D.M., Stoy, P.C., Suyker, A.E., Verma, S.B., Wofsy, S. C., 2006. A multi-site analysis of random error in tower-based measurements of carbon and energy fluxes. Agric. For. Meteorol. 136, 1–18.
Santanello, J.A., Friedl, M.A., 2003. Diurnal covariation in soil heat flux and net radiation. J. Appl. Meteorol. 42, 851–862.
Sánchez, J.M., López-Urrea, R., Doña, C., Caselles, V., González-Piqueras, J., Niclòs, R., 2015. Modeling evapotranspiration in a spring wheat from thermal radiometry: crop coefficients and E/T partitioning. Irrigation. Sci. 33, 399–410.
Scanlon, T.M., Kustas, W.P., 2010. Partitioning carbon dioxide and water vapor fluxes using correlation analysis. Agric. For. Meteorol. 150, 89–99.
Scanlon, T.M., Kustas, W.P., 2012. Partitioning evapotranspiration using an eddy covariance-based technique: improved assessment of soil moisture and land–atmosphere exchange dynamics. Vadose Zone J. 11 (3).
Seguin, B., Becker, F., Phulpin, T., Gu, X.F., Guyot, G., Kerr, Y., King, C., Lagouarde, J.P., Ottlé, C., Stoll, M.P., Tabbagh, A., Vidal, A., 1999. IRSUTE: a minisatellite project for land surface heat flux estimation from field to regional scale. Remote Sens. Environ. 68, 357–369.
Seneviratne, S.I., Corti, T., Davin, E.L., Hirschi, M., Jaeger, E.B., Lehner, I., Orlowsky, B., Teuling, A.J., 2010. Investigating soil moisture–climate interactions in a changing climate: a review. Earth-Sci. Rev. 99, 125–161.
Song, L., Liu, S., Zhang, X., Zhou, J., Li, M., 2015. Estimating and validating soil evaporation and crop transpiration during the HiWATER-MUSOEXE. IEEE Geosci. Remote Sens. 12, 334–338.
Song, L., Liu, S., Kustas, W.P., Zhou, J., Xu, Z., Xia, T., Li, M., 2016. Application of remote sensing-based two-source energy balance model for mapping field

surface fluxes with composite and component surface temperatures. Agri. For. Meteorol. http://dx.doi.org/10.1016/j.agrformet.2016.01.005.
Tanner, C.B., Jury, W.A., 1976. Estimating evaporation and transpiration from a row crop during incomplete cover. Agron. J. 68, 239–243.
Wang, J., Zhuang, J., Wang, W., Liu, S., Xu, Z., 2015. Assessment of uncertainties in eddy covariance flux measurement based on intensive flux matrix of HiWATER-MUSOEXE. IEEE Geosci. Remote Sens. 12, 259–263.
Wen, X.-F., Lee, X., Sun, X.-M., Wang, J.-L., Hu, Z.-M., Li, S.-G., Yu, G.-R., 2012. Dew water isotopic ratios and their relationships to ecosystem water pools and fluxes in a cropland and a grassland in China. Oecologia 168, 549–561.
Wen, X., Yang, B., Sun, X., Lee, X., 2016. Evapotranspiration partitioning through in-situ oxygen isotope measurements in an oasis cropland. Agric. For. Meteorol. http://dx.doi.org/10.1016/j.agrformet.2015.12.003.
Williams, D.G., Cable, W., Hultine, K., Hoedjes, J.C.B., Yepez, E.A., Simonneaux, V., Er-Raki, S., Boulet, G., de Bruin, H.A.R., Chehbouni, A., Hartogensis, O.K., Timouk, F., 2004. Evapotranspiration components determined by stable isotope, sap flow and eddy covariance techniques. Agric. For. Meteorol. 125, 241–258.
Wu, W., Hall, C.A.S., Scatena, F.N., Quackenbush, L.J., 2006. Spatial modelling of evapotranspiration in the Luquillo experimental forest of Puerto Rico using remotely-sensed data. J. Hydrol. 328, 733–752.
Xu, Z., Liu, S., Li, X., Shi, S., Wang, J., Zhu, Z., Xu, T., Wang, W., Ma, M., 2013. Intercomparison of surface energy flux measurement systems used during the HiWATER-MUSOEXE. J. Geophys. Res.: Atmos. 118, 13, 140–13, 157.
Yang, Y., Scott, R., Shang, S., 2013a. Modeling evapotranspiration and its partitioning over a semiarid shrub ecosystem from satellite imagery: a multiple validation. J. Appl. Remote Sens. 7 (1), 073459.
Yang, Y., Guan, H., Hutson, J.L., Wang, H., Ewenz, C., Shang, S., Simmons, C.T., 2013b. Examination and parameterization of the root water uptake model from stem water potential and sap flow measurements. Hydrol. Process. 27, 2857–2863.
Yang, Y., Long, D., Guan, H., Liang, W., Simmons, C., Batelaan, O., 2015. Comparison of three dual-source remote sensing evapotranspiration models during the MUSOEXE-12 campaign: revisit of model physics. Water Resour. Res. 51, 3145–3165.
Zhang, Y., Peña-Arancibia, J.L., McVicar, T.R., Chiew, F.H.S., Vaze, J., Liu, C., Lu, X., Zheng, H., Wang, Y., Liu, Y.Y., Miralles, D.G., Pan, M., 2016. Multi-decadal trends in global terrestrial evapotranspiration and its components. Sci. Rep. 6, 19124.
Zhang, Y., Shen, Y., Sun, H., Gates, J.B., 2011. Evapotranspiration and its partitioning in an irrigated winter wheat field: a combined isotopic and micrometeorologic approach. J. Hydrol. 408, 203–211.
Zhou, J., Li, M., Liu, S., Jia, Z., Ma, Y., 2015a. Validation and performance evaluations of methods for estimating land surface temperatures from ASTER data in the middle reach of the Heihe River Basin, Northwest China. Remote Sens. 7 (6), 7126–7156.
Zhou, J., Li, M., Liu, S., Song, L., 2015b. Deriving soil and vegetation temperatures of a dynamically developing maize field from ground thermal images recorded during the HiWATER-MUSOEXE. In: IEEE International Geoscience and Remote Sensing Symposium (IGRASS). IEEE, Milan, pp. 1725–1728.
Zhu, G., Li, X., Su, Y., Zhang, K., Bai, Y., Ma, J., Li, C., Hu, X., He, J., 2014. Simultaneously assimilating multivariate data sets into the two-source evapotranspiration model by Bayesian approach: application to spring maize in an arid region of northwestern China. Geosci. Model. Dev., 1467–1482